AGU PUBLICATIONS

Geophysical Research Letters

RESEARCH LETTER
10.1002/2017GL076054

Special Section:
New Understanding of the Solar Eclipse Effects on Geospace: The 21 August 2017 Solar Eclipse

Ionospheric Bow Waves and Perturbations Induced by the 21 August 2017 Solar Eclipse

Shun-Rong Zhang[1], Philip J. Erickson[1], Larisa P. Goncharenko[1], Anthea J. Coster[1], William Rideout[1], and Juha Vierinen[2]

[1] MIT Haystack Observatory, Westford, MA, USA, [2] Department of Physics and Technology, University of Tromsø, Tromsø, Norway

Key Points:
- The first unambiguous evidence of eclipse-induced ionospheric bow waves in differential TEC is shown
- The bow waves have 350/270 km wavelength in zonal/meridional directions, and a 25 min period
- They propagate at 280 m/s phase velocity in a direction approximately aligned with the totality path.

Correspondence to:
S.-R. Zhang,
shunrong@mit.edu

Citation:
Zhang, S.-R., Erickson, P. J., Goncharenko, L. P., Coster, A. J., Rideout, W., & Vierinen, J. (2017). Ionospheric bow waves and perturbations induced by the 21 August 2017 solar eclipse. *Geophysical Research Letters*, *44*. https://doi.org/10.1002/2017GL076054

Received 13 OCT 2017
Accepted 30 NOV 2017
Accepted article online 4 DEC 2017

Abstract During solar eclipses, the Moon's shadow causes a large reduction in atmospheric energy input, including not only the stratosphere but also the thermosphere and ionosphere. The eclipse shadow has a supersonic motion which is theoretically expected to generate atmospheric bow waves, similar to a fast-moving river boat, with waves starting in the lower atmosphere and propagating into the ionosphere. However, previous geographically limited observations have had difficulty detecting these weak waves within the natural background atmospheric variability, and the existence of eclipse-induced ionospheric waves and their evolution in a complex coupling system remain controversial. During the 21 August 2017 eclipse, high fidelity and wide coverage ionospheric observations provided for the first time an oversampled set of eclipse data, using a dense network of Global Navigation Satellite System receivers at ~2,000 sites in North America. We show the first unambiguous evidence of ionospheric bow waves as electron content disturbances over central/eastern United States, with ~1 h duration, 300–400 km wavelength and 280 m/s phase speed emanating from and tailing the totality region. We also identify large ionospheric perturbations moving at the supersonic speed of the maximum solar obscuration which are too fast to be associated with known gravity wave or large-scale traveling ionospheric disturbance processes. This study reveals complex interconnections between the Sun, Moon, and Earth's neutral atmosphere and ionosphere and demonstrates persistent coupling processes between different components of the Earth's atmosphere, a topic of significant community interest.

Plain Language Summary During solar eclipses, the Moon's shadow causes a large reduction in atmospheric energy input, including the stratosphere and both the thermosphere and ionosphere (~100–1,000 km altitudes). Theoretical studies since the 1960s have predicted that the Moon's supersonic shadow should generate atmospheric bow waves, similar to a fast-moving river boat. However, observations were geographically limited for these weak and complicated waves. In 2017, high fidelity and wide coverage ionospheric observations were made using a North American Global Navigation Satellite System (GNSS) ~2,000 receiver network. Eclipse passage generated clear ionospheric bow waves in electron content disturbances emanating from totality primarily over central/eastern United States. Study of wave characteristics reveals complex interconnections between the Sun, Moon, and Earth's neutral atmosphere and ionosphere.

1. Introduction

The supersonic motion of the Moon shadow has been thought for some time to induce middle atmospheric perturbations and excite atmospheric acoustic and gravity waves, due to sudden cooling and heating of the atmosphere at altitudes where the ozone layer and water vapor efficiently convert solar UV radiation to heat. Waves generated in this fashion at middle atmospheric altitudes of 10–60 km can propagate upward to the ionosphere at 200–500 km altitude (Chimonas, 1970; Chimonas & Hines, 1971). Comprehensive theoretical treatments of eclipse effects on the middle and upper atmosphere have consistently produced predictions of bow wave generation, but results have also implied that large-scale waves triggered by shadow passage might be weak and difficult to detect at ionospheric altitudes (Fritts & Luo, 1993). Studies also predicted that bow waves should only appear at later times during eclipse recovery, when gravity waves generated in the stratosphere were given sufficient time to propagate vertically (Beer et al., 1976; Eckermann et al., 2007). Some studies also suggested that waves could be generated directly in the thermosphere

(Muller-Wodarg et al., 1998). Observational searches for solar eclipse-induced ionospheric signatures have previously reported traveling ionospheric disturbances (TIDs) with ~20 min periodicity located at distances of a few thousand kilometers behind totality and occurring 1 h after totality passage during the 7 March 1970 eclipse (Davis & Rosa, 1970). However, as summarized by Eckermann et al. (2007, and references therein), some observations reported null detections of eclipse-induced TIDs (Schodel et al., 1973), whereas others reported ionospheric oscillations, consistent with gravity wave scenarios, but with inconsistent source regions either in the stratosphere or thermosphere (Bertin et al., 1977). The study of J. Y. Liu et al. (2011) claimed detection of bow waves and stern waves but was based on significantly limited coverage GNSS TEC data over East Asia during the 22 July 2009 eclipse. In general, this diversity of previous results may be attributed partially to complexities introduced by geomagnetic and other disturbances, limitations related to sparse spatial observation coverage, distance from the totality zone, and instrumental characteristics which could have significantly attenuated apparent signatures of atmospheric waves.

The 21 August 2017 provided a modern and unique opportunity to examine eclipse-induced ionosphere bow waves and disturbances through coupling in altitude from the lower atmosphere to upper thermosphere and between neutral and plasma gases. In particular, the 2017 eclipse totality path traversed the central part of the continental United States (CONUS) with a dense set of ground-based ionospheric sensors. ~2,000 GNSS receivers with millions of transionospheric lines of sight were available to address persistent and challenging eclipse wave generation questions.

2. Observation and Method

We analyzed ionospheric total electron content (TEC) data obtained from these observations on 21 August 2017 during the eclipse period. Ionospheric disturbances are detected by analysis of differential TEC values. Historically, a wide range of GNSS TEC-based studies have uncovered numerous sources of ionospheric disturbances including solar storms and meteorological processes; cf. Azeem et al. (2015), Ding et al. (2007), Saito et al. (1998), and Tsugawa et al. (2007).

The GNSS processing algorithms that produce TEC were developed at MIT Haystack Observatory (Rideout & Coster, 2006; Vierinen et al., 2016). The accuracy of this method is based on the accuracy of the GNSS phase measurement, which is less than 0.03 TEC units (Coster et al., 2012), as all satellite and receiver bias terms cancel out in a differential sense. For detection of TIDs, differential TEC was derived by subtracting a background TEC variation determined by a low-pass-filtering procedure using the Savitzky-Golay low-pass filter approach (Savitzky & Golay, 1964). This algorithm uses a convolution process with least squares fitting of successive subsets of 30 min length involving time-adjacent TEC data points from the same GNSS satellite-receiver pair of data segments. A linear basis function set was used.

Figure 1 shows a sample map of differential TEC derived with the above mentioned background removal procedure for 18:00 UT during the eclipse. It also illustrates the dense distribution of data over the CONUS. Prominent ionospheric depletion in the differential TEC and its spatial extent is evident, and this study's analysis uses this information for its findings.

3. Bow-Shaped TEC Depletion Distribution and Motion

The 21 August 2017 solar eclipse visible in CONUS started with a partial eclipse at 1604 UT (first contact, C1) over Oregon and ended at 20:10 UT (fourth contact, C4) over South Carolina. Corresponding totality events happened between 17:16 UT and 18:49 UT. Figure 2 shows the totality path (TP) with dotted lines, local noon with red lines, and the location of instantaneous totality with white dots. Detected differential TEC show an evident depression front, ahead of and much larger in size than the totality shadow (TS). This bent/bow front (hereafter FR1, Figure 2a) appeared first near Oregon, then moved across the CONUS approximately along the TP and exited from South Carolina (Figure 2e). Depletions were driven primarily from decreases in the lower *F* region and *E* region photoionization and associated dynamic and photochemical responses in the F_2 region (Rishbeth, 1968). The speed and other properties of the front labeled FR1 were estimated using keograms (Figure 3), which alternately plot time variations along a fixed longitude (95°W) and fixed latitude (39°N). The large blue region in each keogram corresponded to the depletion front FR1. The keograms reveal an asymmetric response, in that the FR1 front speed in the zonal direction at W_1 ~700 m/s (the same as the zonal speed of totality and of the maximum solar obscuration at 40°N latitude) but speed in the meridional direction was 2.5 times as fast (1,800 m/s, the same as the speed of the maximum solar obscuration in the 95°W meridional direction).

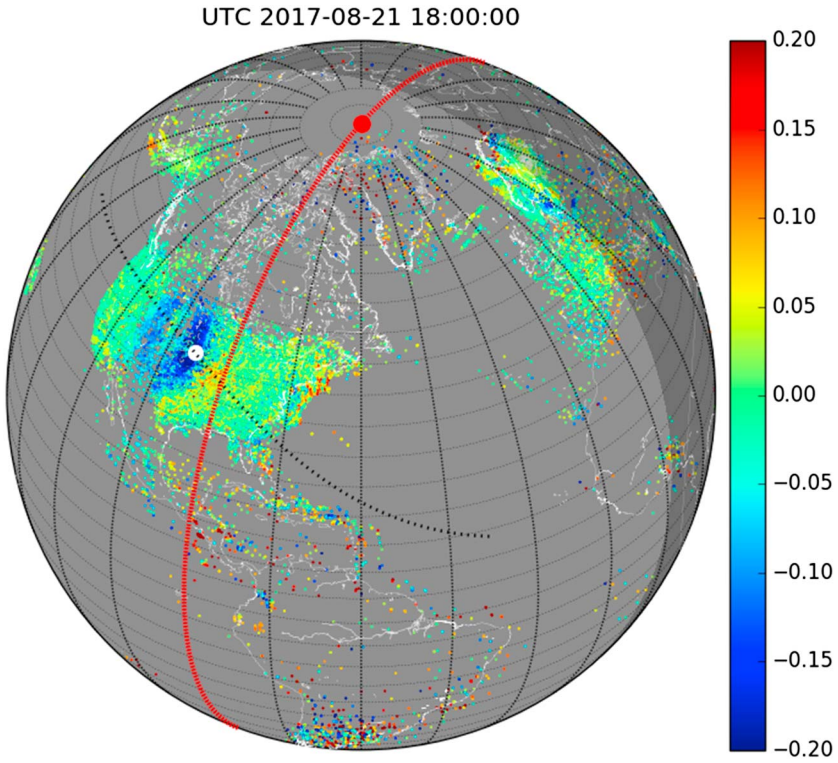

Figure 1. A sample GNSS differential TEC map derived with a background removal procedure, cf. section 2, for 18:00 UT during the eclipse. The map shows also high spatial resolution and wide coverage ionospheric observations which have been available for the first time for an eclipse study. The dotted line indicates the solar totality path, and the white dot gives the location of the totality at 18:00 UT (the true size of the totality shadow is approximately 100 km width, as represented approximately by the size of the white dot). The red line indicates the local noon meridian.

4. Ionospheric Bow Waves

Associated with the moving FR1 front, a clearly visible and observationally oversampled bow wave pattern initially appeared in TEC data at ~18:10 UT in the central United States near local noon. Figure 2b shows well-organized ripple-like waves with largest amplitude near and to the south of the totality zone. As these waves moved southeast, they evolved into higher-amplitude ripples near and on each side of the totality zone (18:27 UT in Figure 2c). A set of "V-shaped" resulting wave fronts developed on the afternoon side at ~18:38 UT (Figure 2d). Note that the Moon totality shadow had ~100 km width, but the penumbra had a diameter of ~3,500 km, and the observed bow waves were well within the penumbra. Bow waves existed for at least 60 min between 18:10 and 19:10 UT over the central and eastern United States and eventually faded into large-scale ionospheric perturbations moving toward the southeast. In fact, Figure 2a depicts partial bow waves developed near 90°W between 30 and 40°N at 17:18 UT when the eclipse magnitude was ~50%. Keogram Figure 3b shows signatures of these weak bow waves between 17:00 and 18:00 UT, with similar wave properties to those strong ones right after totality (18:10–19:10 UT).

Additional keogram analysis in Figures 3a and 3b shows that the bow wave zonal wavelength was ~350 km and zonal propagation speed W_z ~240 m/s, with a wave propagation zonal period of ~25 min. The meridional spatial wave length was ~270 km with a southward propagation speed W_s ~150 m/s and a similar meridional wave period of ~25 min. The results indicate that the wave ripples were not completely circular but elliptical and were indeed bow shaped, traveling at ~280 m/s with a directional azimuth of ~ 122°, close to but slightly farther south of the totality path azimuth (116°) in the eastern United States. The additional azimuth rotation toward the meridional direction is likely an effect of reduced wave filtering along the magnetic field (C. H. Liu & Yeh, 1969) which is mostly in the meridional direction. Nevertheless, in general, these results suggest a very strong correlation between bow wave propagation and totality motion. The bow wave properties of small wavelength and short period imply that the disturbance source region is at a short distance away, most likely within totality or nearby partial eclipse.

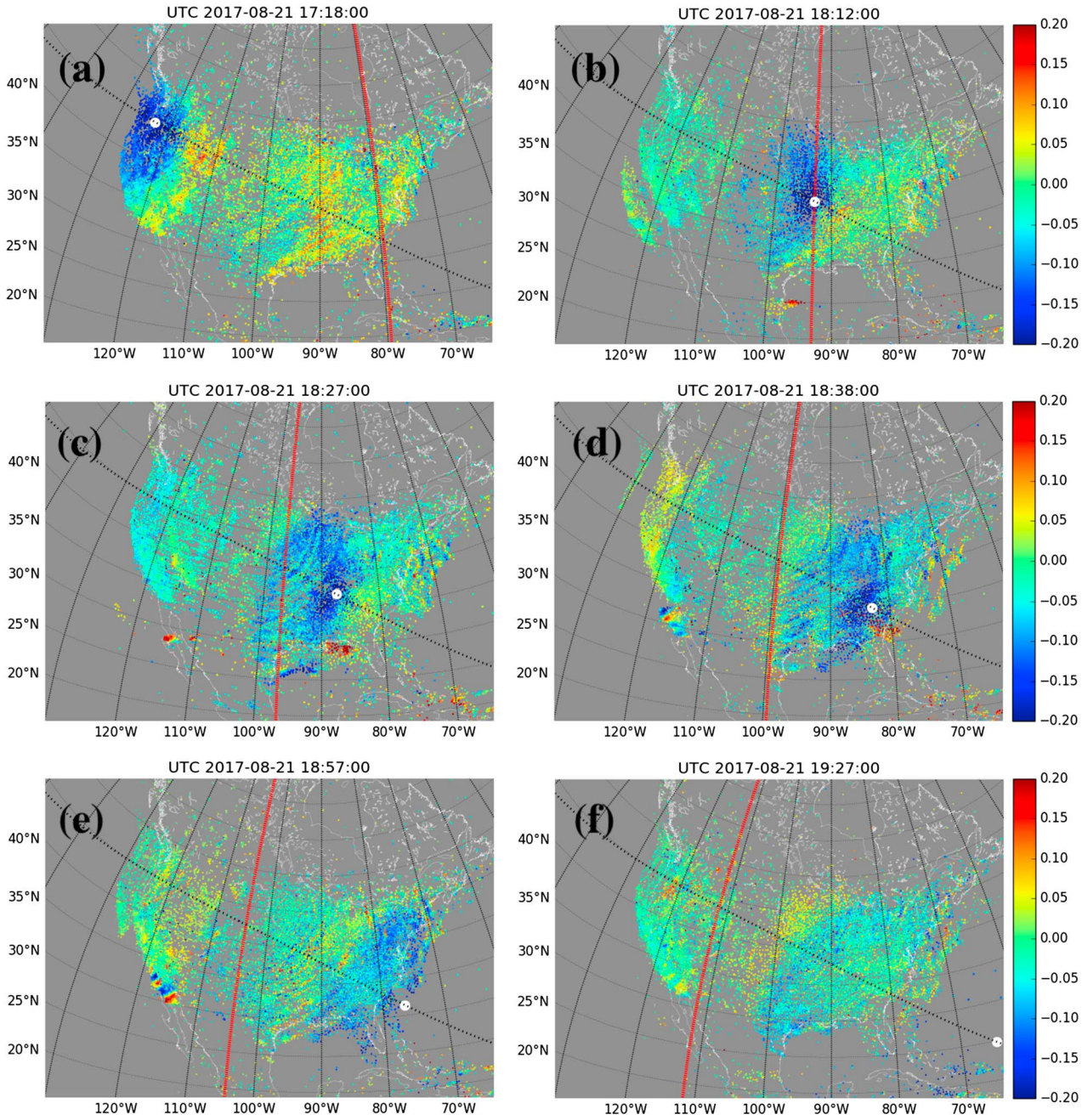

Figure 2. Bow wave evolution as shown by differential TEC (TIDs) (a) at 17:18 UT when the totality was above Oregon, (b) at 18:12 UT when the bow waves occurred initially, (c) at 18:27 UT when the waves appeared as circular perturbations, (d) at 18:38 UT when the waves evolved into "V-shaped" structures, (e) at 18:57 UT when bow waves changed form into plane waves, and (f) at 19:27 UT when totality exited the U.S. coast and the prevailing LSTID waves were decreasing in amplitude. The red line indicates the local noon meridian, and the dotted curve across northwest and southeast of the continental United States shows the eclipse totality path. The white dot indicates the location and size of the totality at the time of the map.

J. Y. Liu (2011) provided the only prior observational finding showing ionospheric bow waves during a solar eclipse period, using GPS TEC data over the south Japan-Taiwan area during the 22 July 2009 solar eclipse. However, the observation was made over a limited field of view in a narrow band during the eclipse passage and showed bow wave-like perturbations in an inherently sparsely sampled region of 15° (longitude) × 5° (latitude). The results also indicated that wavefront curvature was offset by approximately 5° in latitude to the south from the totality (i.e., not trailing the totality as anticipated by Chimonas (1970)) with 20 min periodicity. However, the 21 August 2017 highly oversampled eclipse observations reported here show bow waves that remained centered near the totality track with motion directly along that track and positions that clearly

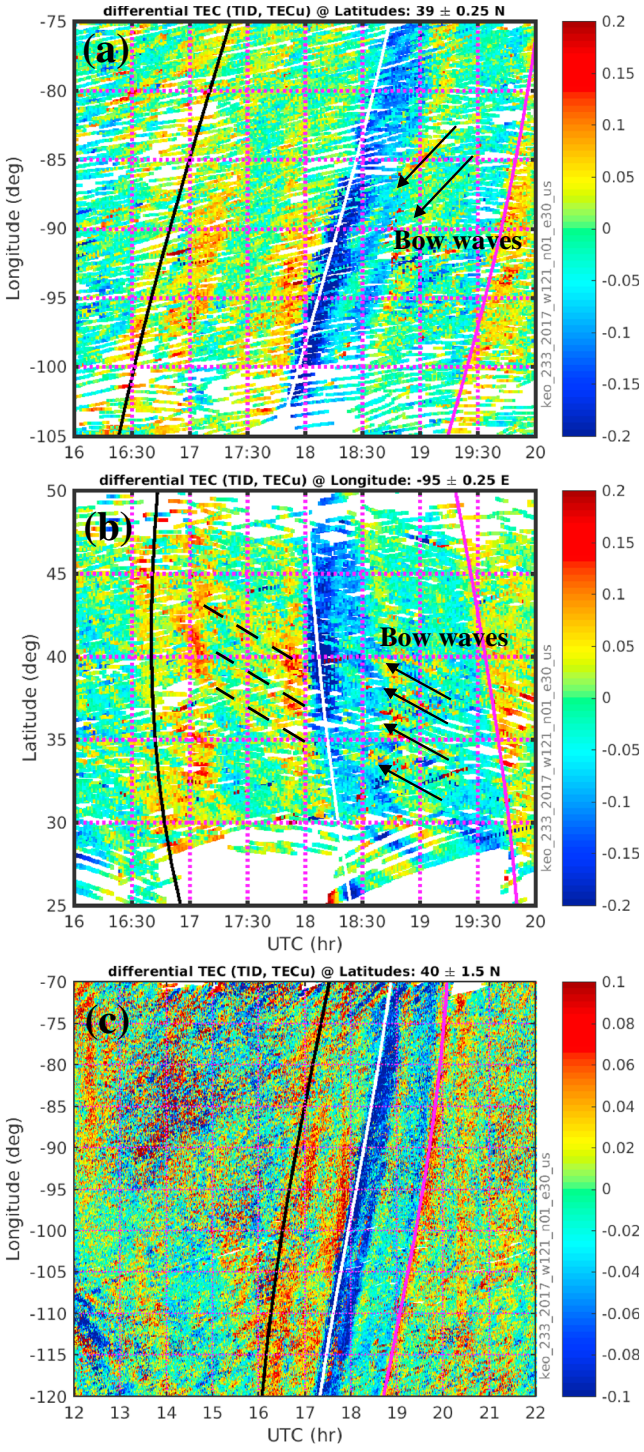

Figure 3. Characteristics of 2017 eclipse bow waves are determined from keograms for (a) a fixed latitude 39°N and (b) a fixed longitude 95°W. (c) The same as Figure 3a but for a longer time span, a larger latitude bin, and a smaller differential TEC scaler range to show large-scale ionosphere perturbations. Black lines indicate the position of the eclipse first contact (C1), the magenta lines are the position of the eclipse fourth contact (C4), and the white lines the position of the largest obscuration. Black arrows and dashed lines in Figures 3a and 3b mark the approximate location of the bow waves.

trailed the totality shadow. These results are in excellent agreement with the theoretical predictions of Chimonas (1970) and provide compelling observational evidence to support the general mechanism of bow wave excitation by the supersonic Moon shadow. (By contrast, ground observation of eclipse-induced gravity wave signatures typically exhibit a range of very different periodicities from ~20 min to a few hours at 100–1,000 km distance from the totality center (Aplin et al., 2016).)

Figure 2d shows that the 2017 eclipse also clearly generated "V-shaped" ionospheric wave fronts as an evolution from earlier elliptically shaped bow waves, in agreement with wave patterns reported in simulations by Eckermann et al. (2007). Furthermore, the wave timing in the 2017 eclipse observations show that the "V-shaped" fronts occurred in a later stage of the eclipse atmospheric response. These bent waves further evolved gradually into large-scale ionospheric perturbations as the eclipse was waning and eventually moved away from the affected region.

5. Large-Scale Perturbations (But Not Truly LSTID Waves)

Separately from eclipse bow waves, TEC eclipse data also clearly show large-scale TEC perturbations that swept the CONUS. These perturbations started at the onset of partial eclipse and disappeared into background ionospheric variations at 20:15 UT as the eclipse moved completely off the U.S. East Coast. These perturbations are readily visible in the keograms of Figure 3c, with the same zonal velocity (~700 m/s) as those from the TEC depletion front FR1 discussed earlier, and the same very large meridional speed (1,800 m/s) as the maximum obscuration speed at 95°W longitude. These have an apparent ~50–60 min periodicity, and ~0.1–0.2 TEC unit (1 TECU = 10^{16} el m^2) amplitudes. Figure 3c also indicates the clear time delay (by ~10 min) between the eclipse totality and the largest TEC depletion. These perturbations, with apparent periodicity and moving characteristics, appear like TIDs, but they are not truly TIDs waves, as further discussed in the following.

TIDs with a wide range of periods, amplitudes, and propagation directions are regularly seen in ionospheric observations and particularly in GNSS TEC data (Azeem et al., 2015; Ding et al., 2007; Saito et al., 1998; Tsugawa et al., 2007). The 2017 eclipse period's observed perturbations were not caused by magnetic activity at high latitudes due to (1) the detailed timing of observed perturbations relative to the eclipse and to prior (before 1500 UT) minor ($Kp \leq 3$) magnetic activity, and (2) a very large TID propagation velocity that could be only produced by the most intense geospace storms which were not in progress at eclipse time. Ionospheric waves excited in the thermosphere during the eclipse were predicted by a previous ionosphere-thermosphere simulation(Muller-Wodarg et al., 1998) but results have a propagation feature (not necessarily oscillatory motion) that is much slower than the supersonic speed observed in the large perturbations during the 2017 event. The 50–60 min apparent periodicity of the perturbations appears consistent with several prior eclipse observations (Altadill et al., 2001; Jakowski et al., 2008). However, the observed speed implies that these perturbations are unlikely to be typical large-scale TIDs (LSTIDs). Specifically, LSTIDs are often thought to manifest as gravity waves in the neutral atmosphere, and these waves should therefore travel at a phase speed less than the sound speed (600–1,000 m/s at 300 km) (Hines, 1960; Yeh & Liu, 1974) and would not be supersonic as seen in the TEC perturbation observations. Figure 3c shows clearly the intensification of ionospheric perturbations between C1 and C4.

Examining carefully the original line-of-sight TEC data, an obvious discontinuity occurred in the TEC variation at C1 and C4. The TEC discontinuity corresponds to the large perturbation fronts in Figure 3 and is most likely a result of immediate ionospheric responses to the sudden onset and end of eclipse modification on the incoming solar irradiation flux. Accordingly, these large perturbations closely followed the motion profile of the maximum solar obscuration region, and ionospheric responses occurred at the characteristic times of eclipse development. The TEC observations during this eclipse, after being filtered using a 30 min sliding window, did not indicate clear continental-size TIDs. Not only in these 30 min sliding window results, the 1 h sliding window results as reported in Coster et al. (2017) also suggested the fast-moving ionospheric perturbations (see the keogram Figure 3 in Coster et al., 2017). It is evident that the perturbations do not change appreciably with the filter time window, and thus, they are not truly waves with a specific period. On the other hand, even though these perturbations are ruled out as eclipse-induced ionospheric waves (TIDs), regional or localized TIDs are still possible, potentially triggered by the eclipse passage; Coster et al. (2017) provided such an example of regional TIDs over the Rocky Mountain region.

Joint bow wave and ionospheric perturbation spatiotemporal analysis allows further conclusions on eclipse effects. In particular, keograms in Figure 3c show that the perturbation front arrived at ~17 UT (C1) first (using, e.g., the 95°W and 35°N location). Later, between 17 and 18 UT, Figure 3b's keogram shows signs of bow waves with propagation properties similar to the most prominent waves between 18 and 19 UT. Another perturbation front at ~18 UT was followed by the large depletion associated with totality. Between 18 and 19 UT, bow wave TIDs became very evident right after totality, but simultaneously with the arrival of the (weak) perturbation front at ~18:45 UT, the bow waves vanished. An hour later (at C4), one additional perturbation front arrived.

In aggregate, the 2017 eclipse bow wave behaviors are generally consistent with many aspects of scenarios suggested in previous theoretical studies (Chimonas & Hines, 1971; Eckermann et al., 2007; Frost & Clark, 2012). In particular, the bow wave propagation velocity is in excellent agreement with these predictions, and their alignment of ~ 122° azimuth is consistent with the totality path of 116° azimuth. These results were obtained using a filter with a 30 min sliding window. Using alternative filters, for example, a 1 h window (with a few different basis functions), to extract differential TEC shows similarly strong signals of bow waves and associated propagation properties.

6. Summary

The unprecedented high fidelity and wide coverage ionospheric observations, provided for the eclipse study by a dense network of GNSS receivers at ~2,000 sites in the CONUS, allow us to determine eclipse-induced ionospheric changes in great details. These observations provide the first unambiguous supporting evidence for eclipse-induced lower atmospheric disturbance processes that eventually appear at ionospheric altitudes as a result of complicated coupling pathways connecting various regions in Earth's atmosphere. Major findings of this study may be summarized as follows: (1) Strong signatures of ionospheric bow waves were identified in the central and eastern United States and were likely associated with eclipse-induced lower atmospheric disturbances; (2) eclipse bow wave characteristics include 350/270 km wavelength in the zonal/meridional direction, 280 m/s phase velocity in a direction approximately aligned with totality, and 25 min period; (3) ionospheric perturbations were immediately intensified at the eclipse first and last contacts, but these perturbations move at supersonic speed and are too fast to be associated with known gravity wave or large-scale traveling ionospheric disturbance processes.

Atmospheric and ionospheric disturbances can be excited by many different sources, ranging from tropospheric convection in the tropics to high-latitude auroral processes. Understanding the ionospheric effects of individual gravity wave and various lower atmospheric perturbation sources remains a challenging research task. The study presented here demonstrates the excellent utility of a modern GNSS-based receiver network for observations of the 2-D temporal evolution of ionospheric waves. The convergence of the predicted and observed interconnections between the different components of Earth's atmosphere represents an important milestone in atmospheric coupling studies. Results present the most comprehensive set of eclipse-induced wave characteristics available to date, advance theoretical understanding, and address a long-standing controversy surrounding one of nature's most spectacular active events.

Acknowledgments
GPS TEC data products and access through the Madrigal distributed data system are provided to the community by the Massachusetts Institute of Technology under support from U.S. National Science Foundation grant AGS-1242204. For eclipse activities, MIT staff members were partially supported by NASA grant NNX17AH71G. In addition, Zhang and Erickson acknowledge NASA LWS funding support (NNX15AB83G); Zhang and Coster acknowledge support from MURI grant ONR15-FOA-0011; and Coster, Zhang, and Goncharenko acknowledge support from ONR N00014-17-1-2186. Data for TEC processing is provided from the following organizations: UNAVCO; Scripps Orbit and Permanent Array Center; Institut Geographique National, France; International GNSS Service; The Crustal Dynamics Data Information System (CDDIS); National Geodetic Survey; Instituto Brasileiro de Geografia e Estatística; RAMSAC CORS of Instituto Geográfico Nacional de la República Argentina; Arecibo Observatory; Low-Latitude Ionospheric Sensor Network (LISN); Topcon Positioning Systems, Inc.; Canadian High Arctic Ionospheric Network; Institute of Geology and Geophysics, Chinese Academy of Sciences, China Meteorology Administration; Centro di Ricerche Sismologiche; Système d'Observation du Niveau des Eaux Littorales (SONEL); RENAG: REseau NAtional GPS permanent; GeoNet, the official source of geological hazard information for New Zealand; GNSS Reference Networks; Finnish Meteorological Institute; and SWEPOS-Sweden. Eclipse timing and location information used in this paper was obtained from www.eclipse-chasers.com with Local Circumstances Calculato (Programmer: Bill Kramer) and also from the data table from the NASA website at https://eclipse.gsfc.nasa.gov/SEpath/SEpath2001/SE2017Aug21Tpath.html (Fred Espinak).

References

Altadill, D., Solé, J. G., & Apostolov, E. M. (2001). Vertical structure of a gravity wave like oscillation in the ionosphere generated by the solar eclipse of August 11, 1999. *Journal of Geophysical Research*, *106*, 21,419–21,428. https://doi.org/10.1029/2001JA900069

Aplin, K. L., Scott, C. J., & Gray, S. L. (2016). Atmospheric changes from solar eclipses. Philosophical Transactions of the Royal Society A: Mathematical. *Physical and Engineering Sciences*, *374*(2077), 20150217.

Azeem, I., Yue, J., Hoffmann, L., Miller, S. D., Straka III, W. C., & Crowley, G. (2015). Multisensor profiling of a concentric gravity wave event propagating from the troposphere to the ionosphere. *Geophysical Research Letters*, *42*, 7874–7880. https://doi.org/10.1002/2015GL065903

Chimonas, G. (1970). Internal gravity-wave motions induced in the Earth's atmosphere by a solar eclipse. *Journal of Geophysical Research*, *75*(28), 5545–5551.

Chimonas, G., & Hines, C. O. (1971). Atmospheric gravity waves induced by a solar eclipse, 2. *Journal of Geophysical Research*, *76*(28), 7003–7005.

Coster, A. J., Goncharenko, L., Zhang, S.-R., Erickson, P. J., Rideout, W., & Vierinen, J. (2017). GNSS observations of ionospheric variations during the 21 August 2017 solar eclipse. *Geophysical Research Letters*, *44*. https://doi.org/10.1002/2017GL075774

Beer, T., Goodwin, G. L., & Hobson, G. J. (1976). Atmospheric gravity wave production for the solar eclipse of October 23, 1976. *Nature*, *264*(5585), 420–421.

Bertin, F., Hughes, K. A., & Kersley, L. (1977). Atmospheric waves induced by the solar eclipse of 30 June 1973. *Journal of Atmospheric and Terrestrial Physics*, *39*(4), 457–461.

Coster, A., Herne, D., Erickson, P., & Oberoi, D. (2012). Using the Murchison Widefield Array to observe midlatitude space weather. *Radio Science*, *47*, RS0K07. https://doi.org/10.1029/2012RS004993

Davis, M. J., & Rosa, A. V. D. (1970). Possible detection of atmospheric gravity waves generated by the solar eclipse. *Nature*, *226*(5251), 1123–1123.

Ding, F., Wan, W., Ning, B., & Wang, M. (2007). Large-scale traveling ionospheric disturbances observed by GPS total electron content during the magnetic storm of 29–30 October 2003. *Journal of Geophysical Research*, *112*, A06309. https://doi.org/10.1029/2006JA012013

Eckermann, S. D., Broutman, D., Stollberg, M. T., Ma, J., McCormack, J. P., & Hogan, T. F. (2007). Atmospheric effects of the total solar eclipse of 4 December 2002 simulated with a high-altitude global model. *Journal of Geophysical Research*, *112*, D14105. https://doi.org/10.1029/2006JD007880

Fritts, D. C., & Luo, Z. (1993). Gravity wave forcing in the middle atmosphere due to reduced ozone heating during a solar eclipse. *Journal of Geophysical Research*, *98*(D2), 3011–3021.

Frost, A. D., & Clark, R. R. (2012). Predicted acoustic gravity wave enhancement during the solar eclipse of June 30, 1973. *Journal of Geophysical Research*, *78*, 3995–3997. https://doi.org/10.1029/JA078i019p03995

Hines, C. O. (1960). Internal gravity waves at ionospheric heights. *Canadian Journal of Physiology and Pharmacology*, *38*, 1441–1481.

Jakowski, N., Stankov, S. M., Wilken, V., Borries, C., Altadill, D., Chum, J., ... Canderd, L. R. (2008). Ionospheric behavior over Europe during the solar eclipse of 3 October 2005. *Journal of Atmospheric and Solar-Terrestrial Physics*, *70*(6), 836–853.

Liu, C. H., & Yeh, K. C. (1969). Effect of ion drag on propagation of acoustic–gravity waves in the atmospheric *F* region. *Journal of Geophysical Research*, *74*(9), 2248–2255.

Liu, J. Y., Sun, Y. Y., Kakinami, Y., Chen, C. H., Lin, C. H., & Tsai, H. F. (2011). Bow and stern waves triggered by the Moon's shadow boat. *Geophysical Research Letters*, *38*, L17109. https://doi.org/10.1029/2011GL048805

Muller-Wodarg, I. C. F., Aylward, A. D., & Lockwood, M. (1998). Effects of a mid-latitude solar eclipse on the thermosphere and ionosphere—A modelling study. *Geophysical Research Letters*, *25*(20), 3787–3790.

Rideout, W., & Coster, A. (2006). Automated GPS processing for global total electron content data. *GPS Solutions*, *10*, 219–228. https://doi.org/10.1007/s10291-006-0029-5

Rishbeth, H. (1968). Solar eclipses and ionospheric theory. *Space Science Reviews*, *8*, 543–554.

Savitzky, A., & Golay, M. J. E. (1964). Smoothing and differentiation of data by simplified least squares procedures. *Analytical Chemistry*, *36*, 1627–1639.

Schodel, J. P., Klostermeyer, J., & Rottger, J. (1973). Atmospheric gravity wave observations after the solar eclipse of June 30, 1973. *Nature*, *245*(5420), 87–88.

Saito, A., Fukao, S., & Miyazaki, S. (1998). High resolution mapping of TEC perturbations with the GSI GPS Network over Japan. *Geophysical Research Letters*, *25*(16), 3079–3082.

Tsugawa, T., Otsuka, Y., Coster, A. J., & Saito, A. (2007). Medium–scale traveling ionospheric disturbances detected with dense and wide TEC maps over North America. *Geophysical Research Letters*, *34*, L22101. https://doi.org/10.1029/2007GL031663

Vierinen, J., Coster, A. J., Rideout, W. C., Erickson, P. J., & Norberg, J. (2016). Statistical framework for estimating GNSS bias. *Atmospheric Measurement Techniques*, *9*, 1303–1312. https://doi.org/10.5194/amt-9-1303-2016

Yeh, K. C., & Liu, C. H. (1974). Acoustic–gravity waves in the upper atmosphere. *Reviews of Geophysics*, *12*(2), 193–216.